Pedestal Temperature Models with Self-Consistent Calculation of Safety Factor and Magnetic Shear

S. Suwanna[1], T. Onjun[1], P. Leekhaphan[1], D. Sukboon[1], P. Thanasutives[1], R. Picha[2], N. Poolyarat[3] and O. Onjun[4]

1) Sirindhorn International Institute of Technology, Thammasat University, Thailand
2) Thailand Institute of Nuclear Technology, Bangkok, Thailand
3) Department of Physics, Thammasat University, Pathumthani, Thailand
4) Department of Science Service, Ministry of Science and Technology, Bangkok, Thailand

e-mail: ssuwanna@siit.tu.ac.th

Abstract. Three pedestal temperature models in the work by T. Onjun *et al* [Phys. Plasma, **9** (2002), 5018] are improved by using self-consistent calculation of safety factor and magnetic shear, acquired directly from the 1.5D BALDUR integrated predictive modeling code. This modification results in an improved estimation of pedestal width and pedestal pressure gradient as the geometrical and bootstrap current effects are properly included. The modified pedestal temperature models are employed together with two core transport models, namely Mixed Bohm/gyro-Bohm and Multimode, to describe the *H*-mode discharges obtained from DIII-D and JET tokamak experiments. For each discharge, profiles of electron temperature and ion temperature from simulations, as well as their values at the top of the pedestal, are compared with the corresponding experimental data from the DIII-D and JET tokamaks. It is found that the predicted pedestal temperature values nearly match the corresponding experimental data, and the profiles yield reasonable agreement with the data near the pedestal, but show high deviation near the plasma-core region. The root-mean-square errors of each profile from each discharge, as well as the offset, are calculated to quantify the agreement.

1. Introduction

A pedestal boundary condition is known to have a strong influence on core density and temperature profiles of tokamak plasma [5]. This condition is especially important for simulating the time-evolution of core temperature and density profiles in *H*-mode plasma because the pedestal or an edge transport barrier can improve the confinement of the core plasma. Moreover, when pedestal boundary conditions are provided, profiles of the *H*-mode discharges can be simulated using the same core transport models as in the *L*-mode discharges, and they have been shown to match experimental profiles reasonably well [4, 6–8], but can be improved with a self-consistent calculation of safety factor and magnetic shear allowing the effect of bootstrap current to be properly included in the pedestal models [6–8].

In typical *H*-mode plasma simulations, the two main components to generate plasma profiles are the core transport models and the pedestal models, which predict temperature boundary conditions at the top of the pedestal. Several core transport models have been developed, most notably the Mixed Bohm/gyro-Bohm (Mixed B/gB) and Multimode (MMM95) transport models [1, 3] which have been implemented in many simulation codes, such as the BALDUR integrated predictive modeling code [9]. Likewise, many pedestal models have been proposed and implemented in recent years [6, 11].

This research is a continuation of our previous work in [10, 12–13], and aims to improve existing pedestal temperature models proposed in [7]. The main improvement targets on the calculation of safety factor and magnetic shear. In this report, the results are based on two different core transport models, namely Mixed B/gB and MMM95, together with three pedestal models whose equations to calculate the pedestal temperature values are included in

Section 2. Our simulation results, including their statistical analysis, will be presented in Section 3, and the conclusions will follow in Section 4.

2. Pedestal Temperature Models

Simulations of the plasma profiles of 26 *H*-modes discharges (14 JETs and 12 DIII-Ds) are performed with the BALDUR integrated predictive modeling code, using the aforementioned transport models. The three scaling width models used in our simulations are derived based on magnetic and flow shear stabilization [$\Delta = C_w \rho s^2$], flow shear stabilization [$\Delta = C_w(\rho R q)^{1/2}$], and normalized poloidal pressure [$\Delta = C_w R(\beta_{\theta,\mathrm{ped}})^{1/2}$] [7, 13]. These scaling width models will be denoted by W01, W02 and W03 respectively, while the Mixed B/gB and MMM95 core transport models will be denoted by T01 and T02 respectively. For instance, the W01T02 combination model will refer to the simulations using MMM95 together with the scaling width model based on flow shear and magnetic shear stabilization.

A detailed description of each scaling width model can be found in [6, 11]. Common ingredients in all scaling width models are the pedestal width (Δ) and the pedestal pressure gradient ($\partial p/\partial r$) [1, 7, 13]. As a result, the pedestal temperature (in keV) can be expressed as

$$T_{\mathrm{ped}} = \frac{1}{2n_{\mathrm{ped}}k}\left|\frac{\partial p}{\partial r}\right|\Delta = \frac{\Delta}{2kn_{\mathrm{ped}}}\frac{\alpha_c B_T^2}{2\mu_0 R q^2},$$

where n_{ped} is the pedestal density (taken from experiment); k is the Boltzmann constant; μ_0 is the permeability of free space; α_c is the normalized critical pressure gradient; B_T is the toroidal magnetic field; R is the major radius; and q is the safety factor. The pedestal pressure gradient is assumed to be uniform throughout the pedestal region [6], and limited by the first stability limit of infinite n ballooning mode, so that the normalized critical pressure gradient (α_c) for the pedestal region is given by $\alpha_c = 0.4s\ [1 + \kappa_{95}^2(1 + 5\delta_{95}^2)]$, where κ_{95} and δ_{95} denote the plasma elongation and triangularity, respectively, at the 95% flux surface. Following [1, 6, 11], the implemented formula for predicting pedestal temperature values in the scaling width models W01, W02 and W03 can be respectively expressed as

$$T_{ped} = C_w^{\,2}\left[\left(\frac{4.57\times10^{-3}}{4\mu_0\left(1.602\times10^{-16}\right)}\right)^2\left(\frac{B_T^{\,2}}{q^4}\right)\left(\frac{A_H}{R^2}\right)\left(\frac{\alpha_c}{n_{ped}}\right)^2 s^4\right] \qquad \text{(W01)}$$

$$T_{ped} = C_w^{\,4/3}\left[\left(\frac{\left(4.57\times10^{-3}\right)^{1/2}}{4\mu_0\left(1.602\times10^{-16}\right)}\right)^{4/3}\left(\frac{B_T}{q}\right)^2\left(\frac{\sqrt{A_H}}{R}\right)^{2/3}\left(\frac{\alpha_c}{n_{ped}}\right)^{4/3}\right] \qquad \text{(W02)}$$

$$T_{ped} = C_w^{\,2}\left[\left(\frac{1}{4\mu_0\left(1.602\times10^{-16}\right)}\right)\left(\frac{B_T}{q^2}\right)^2\left(\frac{R}{a}\right)^2\left(\frac{\alpha_c^{\,2}}{n_{ped}}\right)\left(\frac{\pi q_{95}\left(1+\kappa_{95}\right)}{5g_s}\right)^2\right] \qquad \text{(W03)}$$

where C_w is a constant of proportionality; ρ is the ion gyro radius; s is the magnetic shear calculated at the top of the pedestal; A_H is the average hydrogenic mass; q_{95} is the safety factor at 95% flux surface; and g_s is the geometrical factor. Here, the last two quantities are related by $q_{95} = (5a^2B_T)(\mu_0 I_p R)^{-1}g_s$, where

$$g_s = \frac{[1+\kappa_{95}^{\,2}(1+2\delta_{95}^{\,2}-1.2\delta_{95}^{\,3})](1.17-0.65a/R)}{2\left[1-(a/R)^2\right]^2}.$$

The predictions from BALDUR are compared with the experimental results of DIII-D and JET experiments obtained from the International Profile Database [2]. Following [1], a statistical analysis is performed in individual discharges as well as on a collection of

discharges (e.g. among JET discharges) to compute the root-mean-square (RMS) errors and the offset values to quantify the agreement between simulation and experimental results. The optimal value of C_w is chosen as to minimize the RMS percentages.

3. Results and Discussion

Simulations are carried out in three steps. First, preliminary simulations are carried out in all discharges using MMM95 to verify that the pedestal density values match those from experiments. After matching the pedestal density values, the scaling width models will predict pedestal temperature values, hence providing boundary conditions. Second, simulations are performed in each model to estimate a range of C_w, defined empirically as an interval in which most discharges yield optimal values of C_w with minimum RMS percentages. For both anomalous transport models, the simulations in this step suggest that the range of C_w is between 0.01 and 1.5 in the W01 and W02 width models, whereas the range is between 0.0001 and 0.01 in the W03 model. In the third step, further simulations are carried out in the estimated range of C_w to determine the optimal value of C_w in each combination model.

Considering simulated profiles of electron and ion temperatures, we find that the profiles yield reasonable overall agreement with those from experiments. Generally, the profiles match the corresponding experimental data very well near the pedestal region, but show high deviation near the plasma-core region, see examples in Figure 1. In addition, the electron and ion temperature profiles are plotted as a function of a minor radius near optimal values of C_w, as in Figure 2, to verify that we have obtained a sensible optimal value of C_w and to study trends of deviation away from the pedestal region.

In Tables I–II, the optimal values of C_w and their corresponding minimum RMS percentages from individual discharges are displayed in each combination model. In these tables, missing data points indicate that the simulations do not yield a well-defined minimum point in the estimated range. It can be seen that the optimal values of C_w are distributed between 0.0005–0.002 in the W03 model, which are a few orders of magnitude lower than those in the W01 and W02 models. Figures 3–4 show scatter plots of optimal (C_w, RMS) points for individual discharges in the W01 and W02 width models. In these plots, the discharge numbers should be labeled, but are omitted because they obscure data trends. From Figures 3–4 and Tables I–II, the following trends are observable.

(i) The optimal values of C_w vary significantly from one discharge to another even within the same tokamak; see also Figure 5.

(ii) In the same combination model, the optimal values of C_w for the electron temperature profiles and those for the ion temperature profiles are comparable.

(iii) In each combination model, the simulation results agree very well with explain the experimental results, as the RMS percentage is acceptably low (less than 10% in most discharges, and less than 20 % in nearly all discharges), suggesting that the pedestal temperature models provide reasonably accurate boundary conditions.

(iv) Comparing width models within the same transport model, the values of C_w in the W01 model are greater than those in the W02 model, which in turn are greater than those in the W03 model. However, the minimum RMS values are comparable.

(v) For a given scaling width model, say W01, MMM95 generally yields a more coherent set of optimal C_w values than Mixed B/gB does.

Ultimately, there should be only one value of C_w to represent each scaling width model, which will be termed a *central representative* of C_w. Our simulations show less desirable

outcomes that although each model predicts experimental results in individual discharges very well, it does not accurately predict all discharges with a single value of C_w. Previously many authors have determined a central representative of C_w as to minimize the averaged RMS percentages from all discharges; henceforth, this central representative of C_w will be denoted by C_w*. From Figure 6, our simulations suggest that taking an average of the RMS may not be the best option because the range of optimal C_w is too wide. Moreover, RMS can increase very quickly as C_w varies from its optimal value, for example, in DIII-D discharges. Hence, the averaged RMS value is skewed by high RMS values from only a few discharges, and does not accurately represent agreement between simulations and experiments. On the other hand, in most width models, taking a separate average of RMS in JET and DIII-D discharges seems to provide a moderately accurate central representative of C_w, as seen in the W02 width model shown in Figure 6. However, the minimum averaged RMS percentage is greater than those in most individual discharges. Table III shows the values of C_w*, their corresponding RMS and offset values. It can be observed that, when $C_w = C_w$*, the RMS percentages is less than 26%, but greater than 12%, which is significantly higher than those in most individual discharges.

Consequently, we are confronted with a question as to what should be the best central representative of C_w that will yield the lowest overall RMS percentage and depict low RMS percentages in individual discharges. To that end, we investigate other central representatives, such as a median or a mode, which our simulations indicate that the same problem persists. Taking a weighted average gives rise to the problem of what should be an appropriate set of weights. Alternatively, one may specify an upper bound, say M, of RMS value and find a range of C_w which yields RMS less than M for all discharges. This gives a different measure of how accurate a scaling width model can explain experimental data, as it describes the worst-case scenario of RMS in all discharges. However, our simulations show that all discharges, except JET 37944 and DIII-D 99411, yield at worst 30% RMS when C_w is in the estimated range.

On a possible theoretical improvement, one may modify the current model, for instance, by including the second instability mode region in the calculations or consider other existing pedestal models [7, 13]. All these matters are currently being investigated.

4. Conclusions

The self-consistent simulations of DIII-D and JET tokamak *H*-mode experiments are carried out using the BALDUR integrated predictive modeling code. The results are obtained for ion and electron temperature profiles using the MMM95 and Mixed B/gB core transport models together with three pedestal scaling width models based on flow shear stabilization, flow shear stabilization and normalized poloidal pressure. It is found that simulation profiles yield reasonable agreement with experimental data near the pedestal region, but show high deviation near the core region. Each scaling width model agrees very well with experimental results in individual discharges, but does not seem to explain all discharges within 20% RMS errors with a single constant of proportionality C_w. In addition, a wide range of C_w yields RMS less than 30% in nearly all discharges.

Acknowledgements

This work is supported by Thailand Toray Science Foundation, the Commission on Higher Education (CHE) and the Thailand Research Fund (TRF) under Contract No. RMU5180017.

References

[1] G. Bateman, *et al*, Phys. Plasma, **11** (2003), 4358
[2] D. Boucher, *et al*, Nucl. Fusion, **40** (2000), 1955
[3] M. Erba, *et al*, Plasma Phys. Control. Fusion, **39** (1997), 261
[4] D. Hannum, *et al*, Phys. Plasma, **8** (2003), 964
[5] J. Kinsey, *et al*, Nucl. Fusion, **43** (2003), 1845
[6] T. Onjun, *et al,* Phys. Plasmas, **9** (2002), 5018
[7] T. Onjun, *et al,* Phys. Plasmas, **11** (2004), 1469, 3006
[8] T. Onjun, *et al,* Phys. Plasmas, **12** (2005), 012506, 082513
[9] C.E. Singer, *et al*, Comput. Phys. Commun., **49** (1988), 399
[10] T. Siriburanon, *et al*, TISSAT, **13** (2008), 55
[11] M. Sugihara, *et al,* Nucl. Fusion, **40** (2000), 1743
[12] S. Suwanna, *et al*, Proceeding to the Siam Physics Conference, 2008, Thailand
[13] S. Suwanna, 35th EPS Conference on Plasma Phys., ECA Vol.**32** (2008), P-4.015

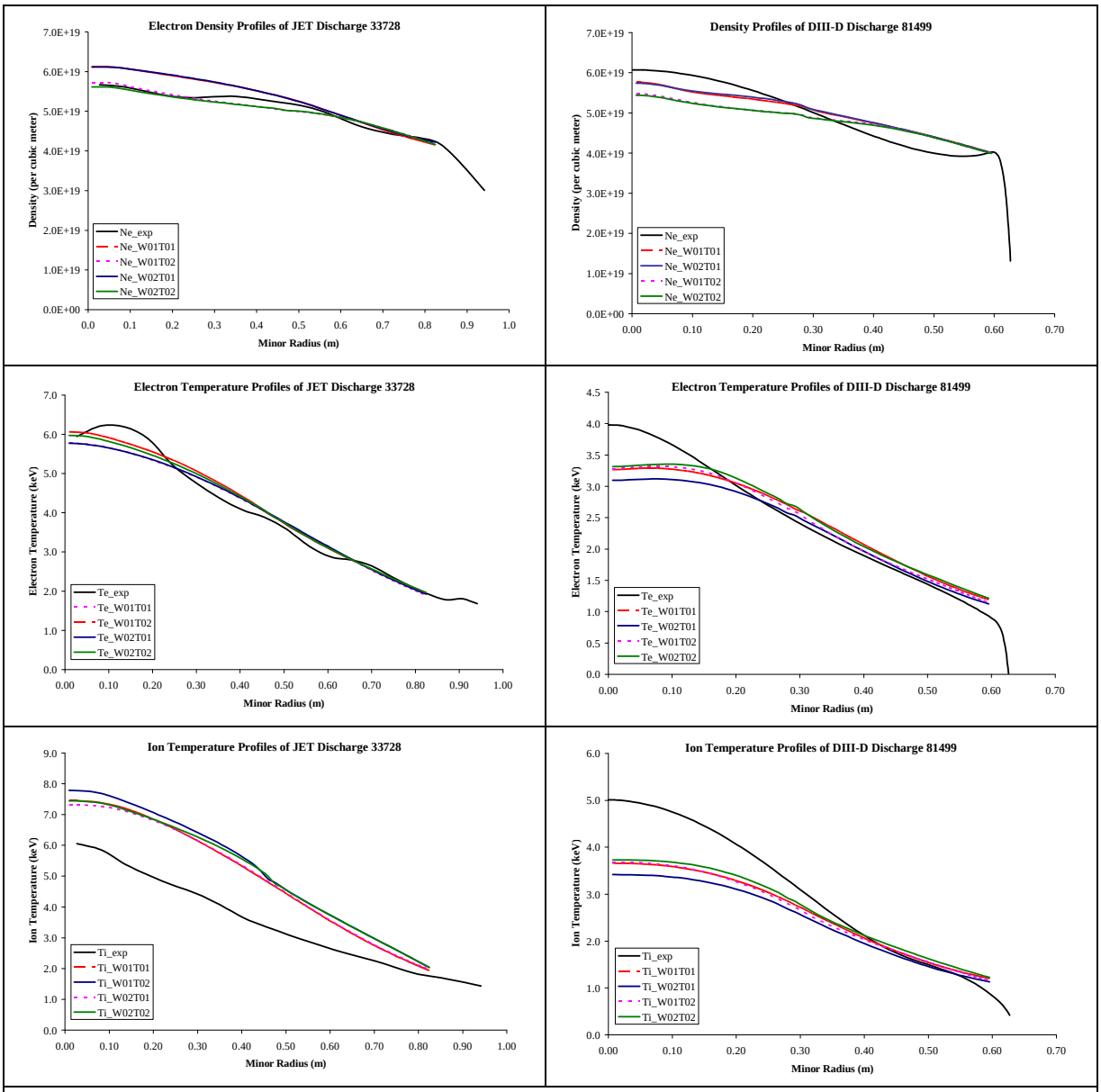

Figure 1: Examples of density, electron temperature and ion temperature profiles, plotted as a function of a minor radius for all considered models. These profiles are plotted near the optimal values of C_w.

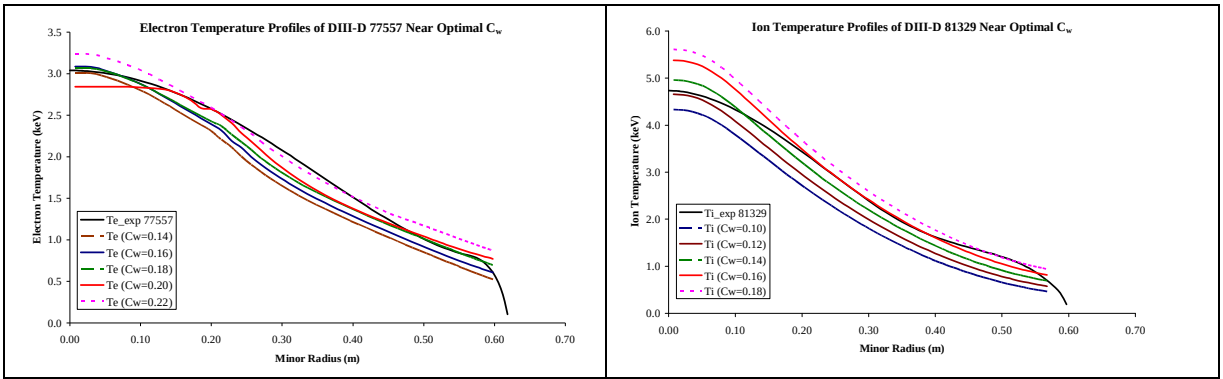

Figure 2: Profiles of electron temperature (left) and those of ion temperature (right) are plotted as a function of a minor radius for values of C_w near the optimal value. These simulations are from the combination models W02T01 and W02T02 respectively.

T01 JET/ DIIID shots	Width Model W01				Width Model W02				Width Model W03			
	Te Profile		Ti Profile		Te Profile		Ti Profile		Te Profile		Ti Profile	
	C_w	RMS (%)	C_w	RMS (%)	C_w	RMS (%)	C_w	RMS (%)	C_w	RMS (%)	C_w	RMS (%)
J32745	0.65	3.1	0.56	10.6	0.16	4.5	0.16	6.8	0.0003	5.5	0.0003	8.0
J33131	0.58	10.7	0.43	13.9	0.20	10.6	0.12	10.0	0.0004	10.1	0.0003	10.3
J33140	0.78	3.5	0.75	2.1	0.20	3.8	0.20	2.9	0.0008	3.8	0.0008	3.6
J33465	0.67	7.6	0.71	6.4	0.16	7.5	0.18	6.3	0.0010	7.8	0.0011	6.4
J34340	1.21	10.0			0.26	7.3	0.36	12.7	0.0007	8.1	0.0008	13.3
J35156					0.36	6.3	0.32	3.5	0.0010	6.6	0.0009	4.7
J35171	0.15	10.1	0.16	11.2	0.06	10.2	0.06	11.8	0.0006	10.3	0.0006	11.6
J35174	0.50	3.9	0.48	4.2	0.18	5.1	0.20	4.9	0.0012	5.4	0.0013	5.3
J37379	1.10	27.9	1.16	28.6								
J37718	0.62	13.1	0.56	10.5	0.18	5.2	0.18	4.0	0.0006	5.6	0.0006	5.5
J37728	0.66	4.2	0.6	6.6	0.22	4.3	0.16	4.6	0.0005	4.9	0.0004	4.3
J38285					0.20	4.9	0.20	3.8	0.0004	5.9	0.0005	4.0
J38287	0.93	19.9	0.93	15.9	0.30	9.8	0.36	3.9	0.0006	14.1	0.0006	9.0
J38407	0.95	4.8	0.95	5.8	0.22	4.9	0.32	6.5	0.0011	6.2	0.0011	7.6
D77557	0.32	4.1	0.40	7.8	0.16	5.0	0.20	8.8	0.0014	5.0	0.0016	8.5
D77559	0.46	5.8	0.54	6.5	0.20	5.4	0.28	7.1	0.0016	5.7	0.0019	8.0
D81321	0.30	6.7	0.42	5.1	0.12	6.7	0.16	5.4	0.0010	6.8	0.0012	5.5
D81329	0.29	4.4	0.28	5.1	0.14	4.4	0.14	4.7	0.0010	4.5	0.0010	5.0
D81499	0.45	8.8	0.52	11.1	0.20	9.4	0.24	11.7	0.0011	9.7	0.0012	11.2
D82183	1.54	7.4	1.80	8.5	0.28	7.4	0.32	8.6	0.0011	7.5	0.0013	8.7
D82188	0.66	5.6	0.70	6.9	0.20	5.7	0.20	7.0	0.0009	5.6	0.0009	7.3
D82205	0.38	8.2	0.40	4.7	0.20	8.6	0.22	5.5	0.0010	8.6	0.0010	5.7
D82788	0.32	5.0	0.50	5.5	0.16	5.0	0.24	5.9	0.0018	5.0	0.0025	5.9
D90108	1.30	10.1	1.44	12.0	0.36	9.8	0.42	11.7	0.0015	9.7	0.0017	11.6
D90117	0.18	5.9	0.38	10.8	0.08	5.8	0.12	11.0	0.0007	5.9	0.0010	11.2
D99411					0.08	25.6	0.08	38.9	0.0007	25.1	0.0008	38.5

TABLE I: Optimal values of C_w in individual discharges in each scaling width model are displayed with their corresponding values of optimal RMS (%). These results are simulated using the Mixed B/gB core transport model (T01).

T02 JET/ DIIID shots	Width Model W01				Width Model W02				Width Model W03			
	Te Profile		Ti Profile		Te Profile		Ti Profile		Te Profile		Ti Profile	
	C_w	RMS (%)	C_w	RMS (%)	C_w	RMS (%)	C_w	RMS (%)	C_w	RMS (%)	C_w	RMS (%)
J32745	0.33	12.1	0.29	19.3	0.12	2.1	0.10	9.3	0.0003	7.4	0.0002	11.2
J33131	0.55	12.4	0.47	7.7	0.14	16.5	0.14	6.0	0.0004	12.9	0.0003	7.0
J33140	0.89	2.7	0.86	3.3	0.20	3.1	0.20	3.4	0.0008	3.1	0.0008	3.9
J33465	0.84	9.9	0.95	7.8	0.20	10.5	0.22	7.8	0.0012	10.4	0.0012	8.0
J34340	1.09	5.0	1.59	12.5	0.20	4.6	0.34	12.6	0.0006	4.1	0.0009	12.4
J35156					0.24	3.8	0.22	8.5	0.0008	4.1	0.0007	8.5
J35171	0.11	16.2	0.14	11.2	0.04	16.1	0.06	10.3	0.0005	15.9	0.0005	11.1
J35174	0.55	4.4	0.58	5.9	0.18	6.9	0.22	8.4	0.0012	6.7	0.0012	9.6
J37379	0.59	3.2	0.66	6.8	0.14	3.8	0.16	6.7	0.0012	3.9	0.0013	6.7
J37718	0.56	15.4	0.51	10.0	0.16	5.6	0.14	4.4	0.0005	6.7	0.0005	4.0
J37728	0.67	3.5	0.58	8.0	0.20	3.7	0.14	5.4	0.0005	3.9	0.0004	6.0
J38285	0.59	17.3	0.64	7.3	0.10	17.4	0.12	7.6	0.0003	18.1	0.0003	7.6
J38287	0.87	20.5	0.84	8.3	0.22	9.8	0.22	2.8	0.0004	13.5	0.0005	7.9
J38407	0.75	4.1	0.7	4.9	0.19	6.1	0.18	7.3	0.0009	5.1	0.0007	5.9
D77557	0.52	5.4	1.08	8.4	0.18	5.7	0.28	9.6	0.0016	5.6	0.0028	8.2
D77559	0.58	6.9	1.00	12.4	0.28	6.6	0.38	11.9	0.0020	6.7	0.0022	9.9
D81321	0.26	5.5	0.32	4.9	0.10	5.9	0.12	4.9	0.0009	5.8	0.0010	4.8
D81329	0.38	4.8	0.36	4.2	0.16	4.5	0.16	3.7	0.0011	4.9	0.0011	4.2
D81499	0.56	8.0	0.62	8.9	0.22	8.6	0.26	9.5	0.0011	8.9	0.0012	9.6
D82183	0.80	10.7	0.80	17.4	0.18	12.8	0.34	17.6	0.0008	10.1	0.0008	17.9
D82188	0.56	8.1	0.52	8.1	0.22	9.3	0.30	9.5	0.0009	9.6	0.0014	8.7
D82205	0.66	11.6	0.78	9.4	0.22	11.6	0.28	9.8	0.0011	11.7	0.0012	9.2
D82788	0.36	5.4	0.46	6.8	0.16	5.6	0.26	6.3	0.0019	5.4	0.0024	6.3
D90108	1.10	6.2	1.28	7.8	0.30	6.2	0.36	7.6	0.0013	6.1	0.0015	7.6
D90117	0.16	4.9	0.28	10.4	0.06	5.0	0.10	9.5	0.0006	5.0	0.0009	9.5
D99411	0.18	15.1	0.22	11.9	0.06	18.7	0.12	12.6	0.0006	13.4	0.0009	12.6

TABLE II: Optimal values of C_w in individual discharges in each scaling width model are displayed with their corresponding values of optimal RMS (%). These results are simulated using the MMM95 core transport model (T02).

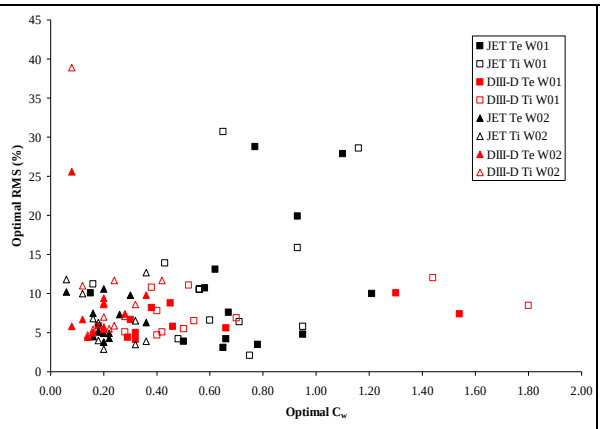

Figure 3: A scatter plot of the optimal values of C_w of temperature profiles from all discharges in W01 and W02 simulated using Mixed B/gB.

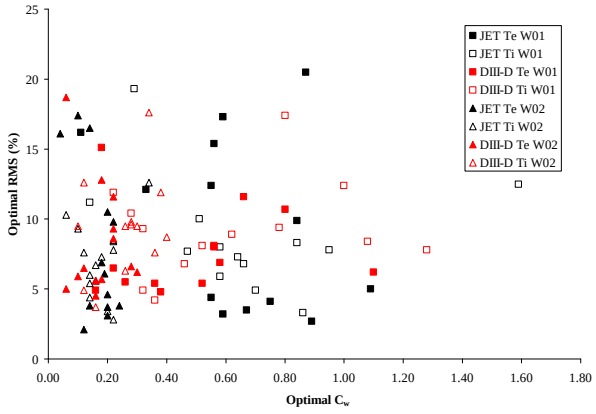

Figure 4: A scatter plot of the optimal values of C_w of temperature profiles from all discharges in W01 and W02 simulated using MMM95.

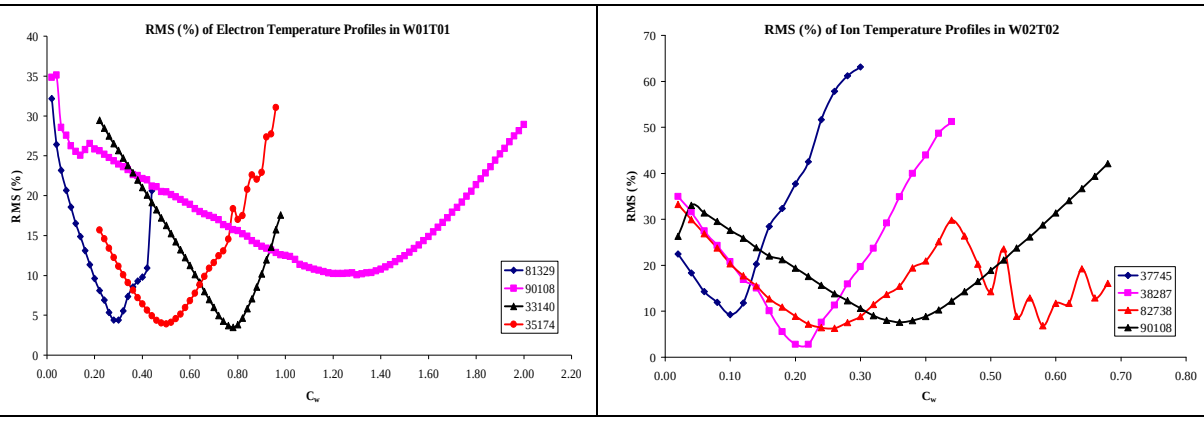

Figure 5: These graphs illustrate that the optimal values of C_w vary significantly from one discharge to another. Some discharges yield multiple values of C_w with comparable RMS percentages.

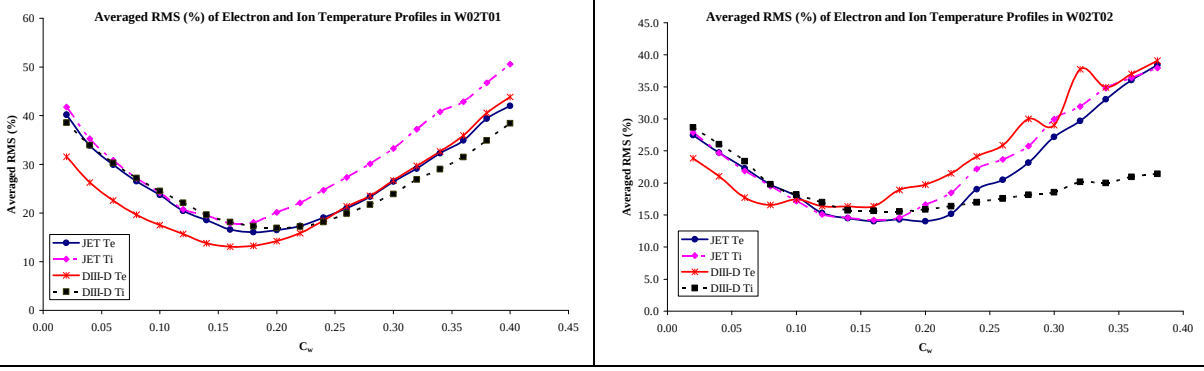

Figure 6: When optimal values of C_w from individual discharges lie in a sufficiently small range, as in the models W02T01 (left) and W02T02 (right), the averaged RMS can be used to determine a single optimal value of C_w which accurately predicts pedestal temperature values in all discharges.

		Mixed B/gB						MMM95					
		W01		W02		W03		W01		W02		W03	
		Te	Ti	Te	Ti	Te	Ti	Te	Ti	Te	Ti	Te	Ti
JET	C_w*	0.44	0.44	0.18	0.16	0.0006	0.0005	0.67	0.62	0.16	0.16	0.0005	0.0004
	RMS %	24.4	25.7	14.3	16.2	17.4	23.5	17.9	16.8	13.2	13.3	17.6	20.1
	Offset	-0.6	-0.6	-0.2	-0.3	0.0	-0.2	0.1	-0.0	-0.1	-0.0	-0.0	-0.3
DIII-D	C_w*	0.36	0.41	0.16	0.20	0.0011	0.0011	0.44	0.46	0.16	0.16	0.0009	0.0011
	RMS %	13.2	16.5	12.4	15.5	12.9	16.5	17.1	16.0	16.9	16.0	15.4	14.5
	Offset	0.1	-0.4	-0.2	-0.3	-0.1	-0.5	0.1	-0.3	0.1	-0.3	-0.1	-0.3

TABLE III: Statistical analysis is performed on simulation results of JET and DIII-D discharges in each combination model. The optimal values of C_w*, and their RMS and offset values are shown.